

AstroSat and *MAXI* view of Cygnus X-1: Signature of an ‘extreme’ soft nature

Ankur Kushwaha^{1,2*}, V. K. Agrawal¹, Anuj Nandi¹

¹Space Astronomy Group, ISITE Campus, U. R. Rao Satellite Centre, Outer Ring Road, Marathahalli, Bangalore, 560037, India

²Department of Physics, Indian Institute of Science, Bangalore, 560012, India

Accepted XXX. Received YYY; in original form ZZZ

ABSTRACT

We present a detailed spectral and timing analysis of Cygnus X-1 with multi-epoch observations, during 2016 to 2019, by *SXT* and *LAXPC* on-board *AstroSat*. We model the spectra in broad energy range of 0.5–70.0 keV to study the evolution of spectral properties while Cygnus X-1 transited from hard state to an extreme soft state via intermediate states in 2017. Simultaneous timing features are also examined by modelling the power density spectra in 3.0–50.0 keV. We find that during high-soft state observations, made by *AstroSat* on Oct 24, 2017 (MJD 58050), the energy spectrum of the source exhibits an inner disk temperature (kT_{in}) of 0.46 ± 0.01 keV, a very steep photon index (Γ) of 3.15 ± 0.03 along with a fractional disk flux contribution of $\sim 45\%$. The power density spectrum in the range of 0.006–50.0 Hz is also very steep with a power-law index of 1.12 ± 0.04 along with a high RMS value of $\sim 25\%$. Comparing the spectral softness of high-soft state with those of previously reported, we confirm that *AstroSat* observed Cygnus X-1 in the ‘softest’ state. The lowest *MAXI* spectral hardness ratio of ~ 0.229 corroborates the softest nature of the source. Moreover, we estimate the spin of the black hole by continuum-fitting method, which indicates that Cygnus X-1 is a maximally rotating ‘hole’. Further, Monte Carlo (MC) simulations are performed to estimate the uncertainty in spin parameter, which is constrained as $a_* > 0.9981$ with 3σ confidence interval. Finally, we discuss the implications of our findings.

Key words: accretion, accretion disks – black hole physics – radiation: dynamics – X-ray: binaries – stars: individual (Cygnus X-1)

1 INTRODUCTION

Black hole X-ray binaries (BH-XRBs) arguably provide wonderful opportunities to understand accretion dynamics. In BH-XRBs, matter from companion star, forms an accretion disk around a black hole. Matter loses angular momentum within disk to viscous dissipation which causes inward drift, heating and emission of radiation. Radiation emanating from disk in proximity to black hole has signatures of strong gravity.

Emission from BH-XRBs can be of thermal and non-thermal origins. The Keplerian accretion disk (Shakura & Sunyaev 1973) is considered to produce multi-colour thermal X-ray emission. Inverse-comptonisation by a ‘hot’ corona (Titarchuk 1994; Tanaka & Lewin 1995; Chakrabarti & Titarchuk 1995) of soft photons emanating from disc, is responsible for higher energy thermal or

non-thermal emission. These two types of emissions are the major components in the energy spectra, of which one component may dominate in a spectral state of BH-XRBs (Remillard & McClintock 2006).

The persistently bright BH-XRBs, in general, exhibit two spectral states, high-soft state and low-hard state whereas spectral states of outbursting BH-XRBs, based on hardness intensity diagram (HID) and spectro-temporal features, can be classified into low-hard state (LHS), hard-intermediate state (HIMS), soft-intermediate state (SIMS) and high-soft state (HSS) (Homan et al. 2001; Homan & Belloni 2005; Remillard & McClintock 2006; Nandi et al. 2012; Radhika et al. 2018; Sreehari et al. 2019; Baby et al. 2020, and references therein).

In HSS, energy spectrum is dominated by thermal emission from disk over Compton tail, while in LHS it is vice-versa (Remillard & McClintock 2006). The thermal emission in HSS is of great importance as it originates in the inner regions of the disk and the spectrum has imprints of inner-disk

* E-mail: ankurksh@urc.gov.in

radius (R_{in}). R_{in} is effectively the inner most stable circular orbit (ISCO) (Tanaka & Lewin 1995; McClintock et al. 2014). The radius of ISCO (R_{ISCO}) is an important parameter which in units of gravitational radii (R_{ISCO}/r_g ; $r_g \equiv GM/c^2$) is a simple function of black hole spin a_* ¹ (Bardeen et al. 1972). Hence, by estimating R_{in} , black hole's spin parameter is measured in BH-XRBs.

Mainly two methods have been developed to estimate the spin of black holes. First method is based on modelling of thermal continuum spectrum of black hole's accretion disk (Zhang et al. 1997; McClintock et al. 2014) and the second method estimates the spin by modelling the profile of a relativistically broadened Fe- K_α fluorescence line (Tanaka et al. 1995; Reynolds 2014). Alternatively, measurement of spin is also possible via high frequency Quasi-periodic Oscillations (HFQPOs) (Abramowicz & Kluźniak 2001; Remillard & McClintock 2006; Dihingia et al. 2019, and references therein) and X-ray polarization (Dovčiak et al. 2008; Schnittman & Krolik 2009) observed in BH-XRBs.

Spin estimation via X-ray continuum-fitting (CF) method requires a disk dominated HSS of BH-XRBs. The thermal disk spectrum, is fitted with thin relativistic disk model `kerrbb` (Novikov & Thorne 1973; Li et al. 2005) and in turn estimates R_{in} of the accretion disk. R_{in} , is then tagged as R_{ISCO} since it is widely accepted that in this state the accretion rate is high enough for the disk to extend to R_{ISCO} , which is related to spin a_* ¹. Accurate measurements of distance (D), mass of black hole (M_{BH}) and inclination angle of the binary plane (i) are crucial in order to determine black hole spin with CF method. In order to reliably estimate the spin with CF method, a geometrically thin disk and a weak Comptonisation of thermal seed photons is preferred. The disk luminosity satisfying a criteria of $L/L_{\text{Edd}} < 30\%$ indicates presence of thin disk (McClintock et al. 2006, 2014). The strength of Comptonising medium is estimated with scattering fraction (f_{sc}), which indicates the fraction of thermal seed photons that is scattered to produce high energy tail. The condition $f_{\text{sc}} < 25\%$ is necessary for successful application of CF method (Steiner et al. 2009b). The method has been employed for many BH-XRBs previously (Gou et al. 2009; McClintock et al. 2014, and references therein) including Cygnus X-1 (Gou et al. 2011, 2014; Kawano et al. 2017), to measure the spin of the black hole.

Cygnus X-1 is a persistent bright high mass X-ray binary with a primary object as confirmed black hole (Webster & Murdin 1972; Bolton 1972) and a massive companion of 09.7 lab type supergiant star HDE 226868 (Walborn 1973). Previously, the binary bf was estimated to be at distance of $1.86^{+0.12}_{-0.11}$ kpc based on radio parallax (Reid et al. 2011) and at 1.81 ± 0.09 kpc based on dust scattering method (Xiang et al. 2011). The mass of the black hole in the binary system was estimated as $M_{\text{BH}} = 14.8 \pm 1.0 M_\odot$ and the inclination of binary plane as $i = 27.1 \pm 0.8$ (Orosz et al. 2011). Recently, Miller-Jones et al. (2021), using VLBA observations, re-estimated the binary system parameters, M_{BH} , i and D to be 21.2 ± 2.2 , $27.51^{+0.77}_{-0.57}$ and $2.22^{+0.18}_{-0.17}$, respectively. Based on the previous parameters, the spin of the black hole, was estimated by Tomsick et al. (2014) as

0.9882 ± 0.0009 (90% confidence level) with Fe- K_α line fitting method using *Suzaku* and *NuSTAR* data. Gou et al. (2014) employed CF method and estimated spin as $a_* > 0.983$ at a confidence level of 3σ (99.7%). Kawano et al. (2017) determined the spin 0.95 ± 0.01 with CF method using data from *Suzaku*. Recently, Zhao et al. (2021), used the updated parameters of binary system and revised the spin parameter as $a_* > 0.9985$ at a confidence level of 3σ .

Cygnus X-1 mostly remains in LHS but displays transitions to HSS. HSS duration can be few months to years (Grinberg et al. 2014). The LHS spectra can be modelled well with Comptonised continuum model. High resolution broad-band spectroscopic observations revealed an additional component attributing to reflection of Comptonised photons from disk (Ling et al. 1983; Parker et al. 2015). Basak et al. (2017) argued for presence of an inhomogeneous Comptonising cloud and suggested two Comptonising components for modelling the spectra. Spectra in HSS, exhibit multi-colour blackbody accountable for accretion disk with steep weak Compton tail. An additional reflection component have also been reported in this state (Gierliński et al. 1999; Tomsick et al. 2014; Walton et al. 2016; Kawano et al. 2017) of the source. Moreover, the broadband spectra of both states have been modelled with two component advective flows model as well Mandal & Chakrabarti (2007).

The short term and long term temporal features and their evolution in different states of Cygnus X-1 have been reported mainly from high time resolution *RXTE* and *AstroSat* observations (Pottschmidt et al. 2003; Axelsson et al. 2005; Grinberg et al. 2014; Misra et al. 2017). The power density spectra (PDS) exhibit multiple broad features which are modelled with multiple Lorentzians. Exception to this are the 'canonical' soft states when one lorentzian plus power-law or only a power-law can successfully represent the PDS (Churazov et al. 2001; Axelsson et al. 2005). During transitions from LHS to HSS, the central frequencies of Lorentzians shift to higher frequencies (Axelsson et al. 2005) but remain below 25 Hz.

Cygnus X-1 has been observed multiple times over last 5 years with *AstroSat*, India's first multi-wavelength space observatory (Agrawal 2006). *AstroSat* was launched on Sept 25, 2015, with five scientific instruments on-board covering a wide range of energies from UV to hard X-rays (Singh et al. 2014; Rao et al. 2016). It provides a unique platform for simultaneous observations, over a wide X-ray band from 0.3 keV to 100 keV, via its suite of co-aligned X-ray instruments - Soft X-ray Telescope (*SXT*) (Singh et al. 2016, 2017), Large Area X-ray Proportional Counter (*LAXPC*) (Yadav et al. 2016b; Antia et al. 2017) and Cadmium Zinc Telluride Imager (*CZTI*) (Vadawale et al. 2016). We exploit the detection capabilities of *SXT* in the soft X-rays to obtain spectra in the lower energies and *LAXPC* enables us to study spectra up to 80 keV. We studied evolution of spectral and temporal properties of Cygnus X-1 over a transition from LHS to HSS via intermediate states (IMS). Cygnus X-1 attains an extreme soft state and we find that during this state source has the 'softest nature' ever observed by any other X-ray observatory. Further, we employ CF method to estimate the spin of the black hole. Since accuracy and success of CF method rely on broadband X-ray observation of BH-XRBs, *AstroSat* data is suitable for such studies. We also

¹ $a_* \equiv Jc/GM_{\text{BH}}^2$, $|a_*| \leq 1$, where J is angular momentum of black hole.

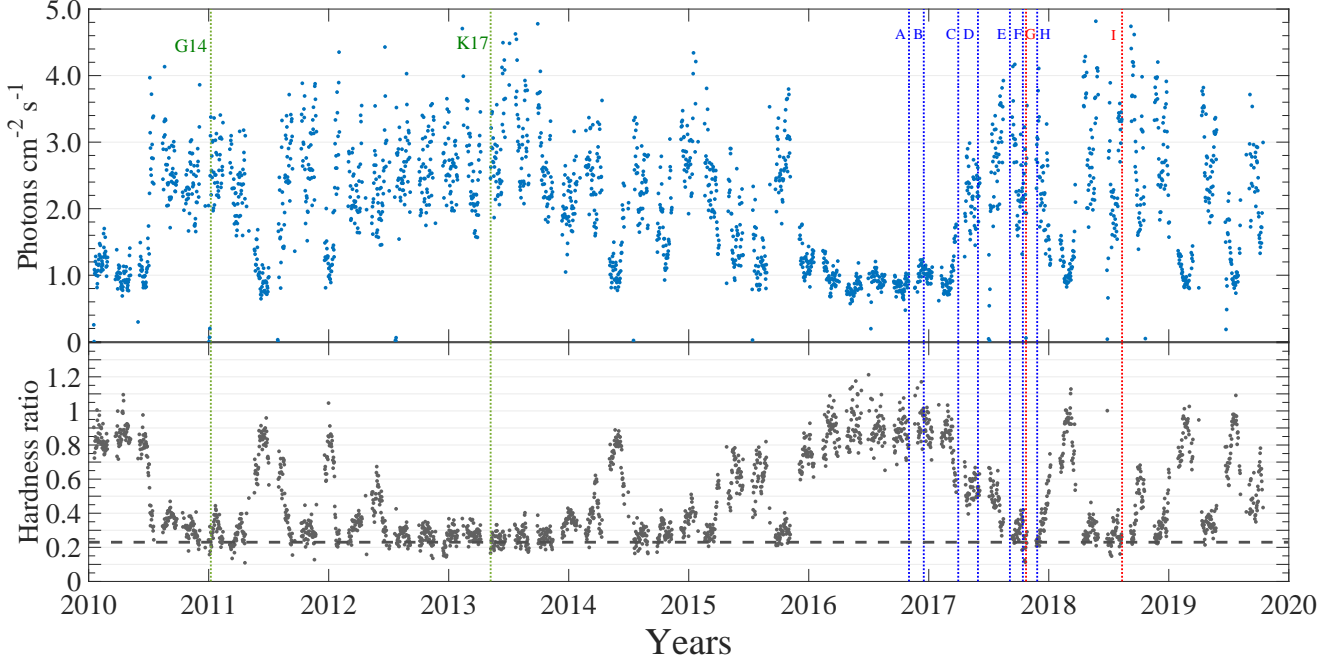


Figure 1. The lightcurve of Cygnus X-1 in the 2.0 – 10.0 keV band (top) and hardness ratio (bottom) based on data obtained using the *MAXI* Gas Slit Camera (GSC; Mihara et al. (2011)). The hardness ratio is defined as the ratio of counts detected in a hard X-ray band (4.0 – 10.0 keV) to those detected in a soft band (2.0 – 4.0 keV). The lightcurve and hardness ratio are day averaged. Green dotted lines denoted with G14 and K17 show previous measurements of spin by Gou et al. (2014) and Kawano et al. (2017). Blue and red dotted lines show *AstroSat* observations along with alphabets corresponding to Table 1, used for this work. Red lines mark the epochs, considered for spin measurement of Cygnus X-1 (see §5). Horizontal black dashed line marks the lowest hardness ratio of 0.229 during *AstroSat* Obs G.

Table 1. *AstroSat* observations of Cygnus X-1 considered in present analysis. From left to right, (1) Name of observation; (2) corresponding *AstroSat* observation ID; (3) spacecraft orbit number since launch date; (4) date of observation; (5) *LAXPC* exposure time; (6) *LAXPC* count rate; (7) *SXT* exposure time; (8) *SXT* count rate. *LAXPC* and *SXT* count rates, provided here, are post data reduction and averaged over exposure time. See §2 for details.

Observation	Obs ID	Orbit	Obs date (MJD)	LAXPC		SXT	
				(ksec)	(counts/sec)	(ksec)	(counts/sec)
Obs A	9000000768	5931	2016 – 11 – 01 (57693)	~ 3.36	~ 1134	~ 2.34	~ 26
Obs B	9000000890	6597	2016 – 12 – 16 (57738)	~ 2.77	~ 1567	~ 0.9	~ 41
Obs C	9000001122	8152	2017 – 03 – 31 (57843)	~ 4.33	~ 1470	~ 1.87	~ 122
Obs D	9000001258	9043	2017 – 05 – 31 (57904)	~ 3.73	~ 1447	~ 1.46	~ 118
Obs E	9000001516	10485	2017 – 09 – 05 (58001)	~ 5.10	~ 1389	~ 2.14	~ 263
Obs F	9000001616	11068	2017 – 10 – 14 (58040)	~ 2.86	~ 1272	~ 1.57	~ 388
Obs G	9000001636	11212, 11215	2017 – 10 – 24 (58050)	~ 3.19	~ 990	~ 1.93	~ 381
Obs H	9000001726	11717	2017 – 11 – 27 (58084)	~ 4.93	~ 1938	~ 2.33	~ 402
Obs I	9000002302	15548	2018 – 08 – 13 (58344)	~ 4.88	~ 1162	~ 2.15	~ 291

make use of the temporal resolution ($\sim 10 \mu\text{s}$) of *LAXPC* to obtain PDS of Cygnus X-1, in order to study the temporal features during the softest state and various phases of accretion states.

In §2, we have given details of the observations and the steps for data reduction. We have discussed broadband spectral analysis using both *SXT* and *LAXPC* data and the results from phenomenological as well as physical modelling in §3. Detailed analysis of PDS has been carried out with *LAXPC* data and the results are presented in §4. We discuss about the ‘softest’ nature of the source and present the details of spin measurement in the softest state with CF

method in §5. Finally, we have discussed the results and have concluded in §6.

2 OBSERVATIONS AND DATA REDUCTION

Cygnus X-1, for the last decade 2010 – 2020, has been showing atypical behaviour of remaining mostly in soft states when compared to previous ~ 15 years (1996 – 2010) where it was typically found in hard state with occasional soft state transitions (Grinberg et al. 2014). Lightcurve obtained from continuous monitoring of source with *MAXI*, clearly shows

this behaviour of the source (see Figure 1). The monitoring shows that the source is in persistent LHS in 2016 and subsequently, in 2017 starts a transition into HSS. We make use of *MAXI* lightcurve in 2.0 – 10.0 keV energy band and hardness ratio (HR) of two energy bands 4.0 – 10.0 keV to 2.0 – 4.0 keV (hereafter *MAXI*-HR) in order to select observations from *AstroSat* data during this transition period (Figure 1).

Cygnus X-1 was observed by *AstroSat* for last 5 years (2016 – 2020) with about ~ 60 co-ordinated pointings. We have selected 9 observations from Guaranteed Time (GT) phase for this work, as our primary goal is to study the broadband characteristics during the transition phase of the source. Hence, we select only those observations which are suitable to study the entire transition from LHS to HSS via IMS during the *AstroSat* campaign. The details of multi-epoch observation logs are provided in Table 1 and also marked in Figure 1. We make use of data from *SXT* and *LAXPC* on board *AstroSat* to carry out broadband spectral and timing analysis on these selected observations.

SXT is a soft X-ray instrument capable of imaging and spectroscopy in the 0.3 – 8.0 keV energy range. *SXT* has a focusing telescope and a charged-coupled device (CCD) detector (Singh et al. 2017). The *SXT* CCD calibration procedures and results are summarized by Singh et al. (2016, 2017). Extraction of level 2 data from *SXT* raw data is done using the *sxtpipeline* tool by *SXT* instrument team² and is available on ISSDC website³ (see also Sreehari et al. 2019; Baby et al. 2020). The *SXT* data are available in the Photon Counting (PC) mode. The extracted cleaned event files are used to generate energy spectra with *XSELECT V2.4d*. Spectra and lightcurve are extracted from an annular region over *SXT* CCD image of the source (see Figure 2). As Cygnus X-1 is a bright source and saturates the central pixels of image location on *SXT* CCD, thus annular source region with inner radius of $\sim 3'$ has been excluded for data extraction to avoid pile-up (see §6, for details on pile-up estimation in *SXT* spectra), while the outer radius varied from 12' – 16' depending on the size of source image in different states and epochs. Smaller outer radii correspond to LHS data sets since counts from source is very low and bigger radii causes high background contribution. The spectra have 1024 channels and for fitting purpose, we use the spectra without rebinning along with the background, response as well as ARF files provided by *SXT* instrument team².

The *LAXPC* is one of the primary instruments on board *AstroSat* and consists of three identical co-aligned X-ray proportional counter units (*LAXPC10*, *LAXPC20* and *LAXPC30*) providing with high time resolution ($\sim 10 \mu\text{s}$) covering 3.0 – 80.0 keV energy band (Yadav et al. 2016b; Antia et al. 2017; Agrawal et al. 2017). All three units are calibrated with Crab observations and further details on the same are given by Antia et al. (2017, 2021). Data from *LAXPC10* unit are unstable, while *LAXPC30* data are not considered due to the continuous gain shift observed in this unit, suspected to be caused by a gas leakage (Antia et al. 2017). Thus, in this work, we use the data only from *LAXPC20*, which is stable and working nominally since

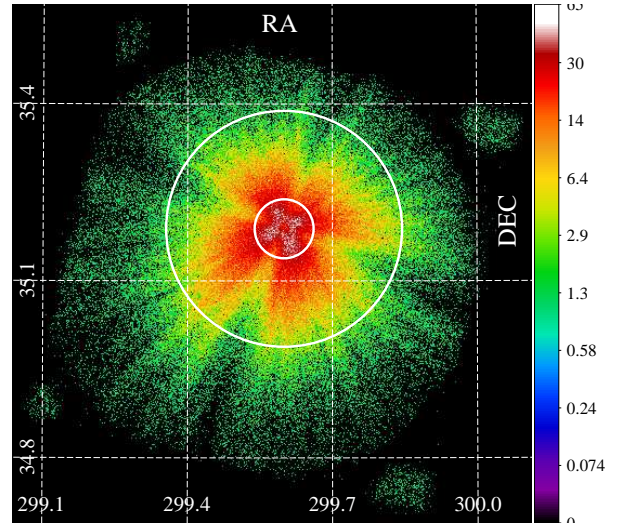


Figure 2. The image of Cygnus X-1 on *SXT* CCD shown in false colors during Oct 24 2017 (MJD 58050) observation. CCD was operated in photon counting (PC) mode. Source photons are extracted within annular region, shown in solid white, with inner and outer radii of 3' and 12', respectively. The region within inner radius is excluded to avoid piled-up events. Calibration source illumination can be seen on four corners of the CCD. The colour bar alongside is for the source intensity in *SXT* (cts pixel⁻¹). See text for details.

launch. A very recent Crab observation with *LAXPC20* is discussed by Antia et al. (2021) where spectral fit parameters are found to be well within the acceptable limits. *LAXPC20* was operated in event analysis (EA) mode during all the observations. The capabilities of *LAXPC* for timing and spectroscopic studies of various sources are already demonstrated by Yadav et al. (2016a); Misra et al. (2017); Verdhan Chauhan et al. (2017); Agrawal et al. (2018); Sreehari et al. (2019); Baby et al. (2020); Agrawal & Nandi (2020); Agrawal et al. (2020); Sreehari et al. (2020).

We followed these papers and the instructions provided along with the *LAXPC* analysis software (*LaxpcSoft*⁴) released on Sept 9, 2019. The details of how the responses and background spectra are generated, are described in Antia et al. (2017). Further, the source and background energy spectra are extracted from events in all layers and anodes of *LAXPC20*. Moreover, only single events are considered for generating the spectra. These options are selected to have a minimal undesired bump in the spectral residuals at around 33 keV which attributes to Xenon fluorescence from detector. The extracted spectra have 256 channels and we use the spectral data for fitting without rebinning. *LaxpcSoft* generates GTI files of good time interval which reduces the data and results in data gaps attributing to South Atlantic Anomaly (SAA) passes and Earth occultations during observations.

² https://www.tifr.res.in/astrosat_sxt/dataanalysis.html

³ <https://www.issdc.gov.in/astro.html>

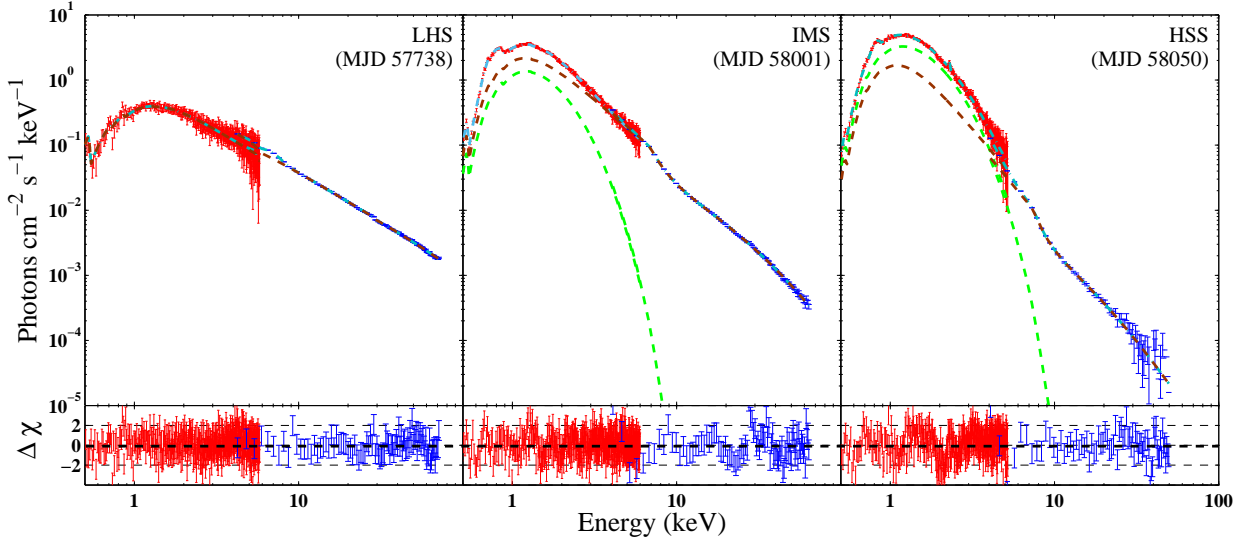


Figure 3. Broadband energy spectra (unfolded) of Cygnus X-1 in LHS (left), IMS (middle) and HSS (right) for Obs B, E & G, respectively. *SXT* and *LAXPC* data is shown in red and blue, respectively. Hard state spectra are fitted with absorbed *nthComp* (dashed brown line). There is an additional *diskbb* component (green dashed line), for the other two states (IMS and HSS). Cyan dotted dash lines show the total model. Bottom panels show the corresponding residuals in units of σ . See the text for details.

3 SPECTRAL ANALYSIS AND RESULTS

We consider broadband modelling of energy spectra obtained during all observations listed in Table 1. *SXT* and *LAXPC* spectra are simultaneously fitted in *HEASoft XSPEC 12.10.0e* package. Energy ranges of 0.5 – 6.0 keV and 4.0 – 70.0 keV have been considered in spectral fit for *SXT* and *LAXPC*, respectively.

We start with Obs A and modeled the spectrum with *Tbabs* (Wilms et al. 2000), *diskbb* (Mitsuda et al. 1984) and *power-law* of *XSPEC*. The relative cross-normalization between the *LAXPC* and *SXT* data is taken care by multiplicative constant factor. The fit gives a very low and unrealistic value of disk temperature though χ^2_{red} of $927.76/643 = 1.44$ indicates a good fit. Hence, we removed the disk component and fitted with *Tbabs* and *nthComp* (Zdziarski et al. 1996). The model gives a χ^2_{red} of $1077.5/645 = 1.67$. The value of kT_{bb} is fixed to a fiducial value of 0.1 keV. We then correct for instrument features at 1.8 and 2.24 keV arising from *SXT*. Also, a broad absorption dip, present at ~ 8 keV, is modelled with *smedge*. An instrumental Xenon edge around 30 keV and 2% systematic uncertainty is introduced in order to achieve a good estimate of the spectral fit parameters (Sreehari et al. 2019). This results into a significantly improved χ^2_{red} value of $848.72/638 = 1.33$. The fit gives model parameters of photon index (Γ) as 1.59 ± 0.01 and electron temperature (kT_e) of $86.94^{+81.89}_{-21.91}$. Unless mentioned explicitly, all the errors are computed using $\Delta\chi^2 = 1.0$ (1σ confidence level) for all the observations. Spectral analysis and fit procedure for Obs B is similar to that of Obs A. The resulting fit parameters are given in Table 2 and the spectra fitted with the model is shown in the left of Figure 3.

The hydrogen column density N_H is estimated to be 7.52×10^{21} atoms cm^{-2} from the fit. This is in good agreement

with estimations of previous investigators (Tomsick et al. 2014; Parker et al. 2015; Walton et al. 2016; Kawano et al. 2017). It is to be noted that HEASARC N_H calculator⁵ gives an average value for hydrogen column density of 7.01×10^{21} atoms cm^{-2} for Cygnus X-1. Xiang et al. (2011) estimates hydrogen column density towards Cygnus X-1 as $N_H \approx 4.65 - 4.85 \times 10^{21}$ atoms cm^{-2} by dust scattering modelling.

Moving onto the softer observations, as indicated by hardness ratio from *MAXI* (see Figure 1 and Table 1), we attempt to fit the spectrum, from Obs C, with *Tbabs* and *nthComp*, but the fit shows residuals below 10 keV, suggesting inclusion of a thermal disk emission component in the model. Hence, *diskbb* is added to model the spectrum. The fit gives a value of 0.29 ± 0.01 for inner disk temperature (kT_{in}) and a disk normalisation of $18.18^{+3.16}_{-2.76} \times 10^4$. The photon index (Γ) is found to be 1.91 ± 0.01 , which suggests the spectrum has become steeper. We note that Obs C marks the advent of soft state transition. Further, similar fit procedure is applied to Obs D and E. The inner disk temperature, during Obs D is slightly higher than that of Obs C and the disk normalization decreases to a value of $12.26^{+2.52}_{-1.80} \times 10^4$. Further, during Obs E, inner disk temperature increases to a value of 0.43 ± 0.01 while the fit gives a disk normalization of $2.94^{+0.28}_{-0.26} \times 10^4$. Photon index (Γ) keeps on increasing, making the spectrum steeper (see middle panel of Figure 3) with values of 1.86 ± 0.01 to 2.28 ± 0.02 for Obs D and Obs E, respectively. Subsequently, spectral fit for Obs F with the same model gives roughly similar values of inner disk temperature and normalization of disk as Obs E. The photon index is even steeper with value of 2.66 ± 0.01 . The spectrum from Obs G is fitted in the same way except the energy range of *LAXPC* is considered from 5.0 keV onwards. The fit results an even higher inner disk temperature of 0.46 ± 0.01 keV.

⁴ https://www.tifr.res.in/~astrosat_laxpc/software.html

⁵ <https://heasarc.gsfc.nasa.gov/cgi-bin/Tools/w3nh/w3nh.pl>

Also, the fit results in higher photon index (Γ) of 3.15 ± 0.03 , which suggests the steepest spectrum of all the observations (see right panel of Figure 3). Fit results into a χ^2_{red} value of $946.08/530 = 1.78$. Additionally, observations Obs H and I are modelled in the same way as mentioned for previous states. The fit parameters of all the observations are summarized in Table 2.

3.1 The Softest Spectral State

The spectral fit parameters obtained in the analysis evidently confirm that the spectral nature of the source evolved from LHS to HSS. Additionally, in order to identify the spectral states of the source, we define criteria based on the inner disk temperature (kT_{in}) and photon index (Γ). We classify observations with $\Gamma < 1.8$ and no disk component, as LHS. Spectra that exhibit Γ between 1.8 – 2.5 along with kT_{in} in range 0.3 – 0.4 keV are identified as IMS. The observations with very steep Γ values in 2.5 – 3.2 and high kT_{in} ranging in 0.4 – 0.5 keV are classified as HSS. Hence, Obs A & B are classified as LHS, Obs C, D & E as IMS and Obs F, G, H & I are of HSS.

Moreover, the spectral fit parameters obtained for observation made by *AstroSat* on Oct 24, 2017 (Obs G, MJD 58050) clearly indicate that Cygnus X-1 exhibits very soft nature as the spectrum has the highest inner disk temperature of 0.46 ± 0.01 and the steepest photon index of 3.15 ± 0.03 . Furthermore, we calculate the disk flux contribution in the total spectrum for all observations. It is found that Obs G spectrum has the largest disk flux contribution of $\sim 45\%$ in net flux in 0.1 – 100.0 keV, which indicates dominance of the disk and major contribution of soft thermal component in the spectrum. These findings evidently suggest that Cygnus X-1 is in extremely soft spectral state. Also, during this observation, we notice that the *MAXI* hardness ratio drops to a very low value of ~ 0.229 (Figure 1), which further corroborates an extreme soft nature of the source. Studying the observed variability of *MAXI* hardness ratio of last 10 years we infer that Cygnus X-1 possibly attains an ‘extreme’ soft state that has ever been recorded. It further motivates us to analyse and study timing properties with *AstroSat* observations.

4 TIMING ANALYSIS AND RESULTS

We track the evolution of temporal features of Cygnus X-1 strictly simultaneous to spectral observations. In order to study temporal features of source in different states, lightcurves of 5 ms resolution from *LAXPC20* data sets in the energy range from 3.0 – 50.0 keV are extracted. Thereafter each lightcurve is divided in multiple intervals of 2^{15} timebins (equivalent to multiple 160 sec long lightcurve segments) and then PDS is generated for each interval. The final PDS for each lightcurve is generated after averaging these individual PDS over entire observation. The averaged PDS is binned by a geometrical factor of 1.05 in frequency space. Normalization for each PDS is similar to that of Belloni & Hasinger (1990); Miyamoto et al. (1992) where PDS is given in units of the squared fractional rms variability per frequency interval. Further, we represent the PDS in units of frequency times power ($f \times P_f$) versus frequency

(Belloni et al. 1997). We consider frequency range upto 50 Hz for modelling as beyond this in higher frequencies data is not reliable and may be affected by dead time correction.

We start with modelling of power density spectra of LHS (Obs A), with three Lorentzians since previous investigators (Pottschmidt et al. 2003; Axelsson et al. 2005; Misra et al. 2017) have shown that PDS of Cygnus X-1 in hard state can be well modelled with multiple Lorentzian profiles. One of the Lorentzians center is fixed to zero to represent broad band limited noise (BLN). This model gives a χ^2_{red} of $154.85/114 = 1.36$. The residuals suggest requirement of a narrow Lorentzian feature below 0.1 Hz. Hence an additional Lorentzian component is added to the model. Fit results in an improved χ^2_{red} value of $144.09/111 = 1.29$. We consider this model as the best fit for LHS and similarly model other PDS of LHS obtained for Obs B. Fit results are shown in Figure 4 (left) and best fit parameters are given in Table 3. We calculate fractional root mean square (RMS) variability by integrating model over frequency range of 0.006–50.0 Hz. An RMS value of $\sim 28\%$ is noted in LHS, of which $\sim 20\%$ contributes to BLN component. Further, PDS of IMS from Obs C and D are fitted with two Lorentzian as power spectra show only two broad features. A χ^2_{red} of $215.57/116 = 1.85$ results from the fit for Obs C. Residuals below 0.2 Hz indicate a need of power-law to further improve the fit. Hence a cut-off power-law is incorporated in existing model which gives a χ^2_{red} of $176.19/113 = 1.54$. Similar fit procedure is applied to PDS from Obs D. We calculate an RMS value of $\sim 20\%$ in PDS for these observations, which is $\sim 8\%$ lesser than that of LHS.

Moving onto softer spectral states observations, we notice that PDS are steep in nature. Hence PDS, obtained from Obs E to Obs H, are modelled with a cut-off power-law. We notice fit for Obs E results in χ^2_{red} of $188.3/119 = 1.58$. The power-law index value is found to be 0.97 ± 0.01 . It is observed that RMS value increases to $\sim 26\%$ when compared that of Obs C & D. Obs F, G & H when fitted with power-law, show residual suggesting presence of BLN component. Addition of BLN component to power-law improves the fit significantly for Obs F & H and fits result in χ^2_{red} values of 1.72 & 1.47, respectively. This improvement is moderate for Obs G with a χ^2_{red} value of 1.32. Overall fit for Obs G is shown in right panel of Figure 4. We notice fits give power-law index close to unity ($\propto f^{-1}$).

Moreover, we observe during Obs G when spectral nature becomes the softest, cut-off power-law index is further steeper with an index of 1.12 ± 0.07 , when compared to that of other observations (Obs F and H) with soft spectral nature. In terms of RMS values Obs F & H have roughly same values of $\sim 28\%$, while Obs G shows a lesser value of $\sim 25\%$. Finally, we calculate the flux variability ($F_{var} = \sqrt{\frac{S^2 - \bar{\sigma}_{err}^2}{\bar{x}}}$, where S^2 , $\bar{\sigma}_{err}^2$ and \bar{x} are the variance, mean square error and arithmetic mean of time series representing lightcurve) for each observation following Vaughan et al. (2003). The calculated F_{var} for various states are presented in Table 3.

Table 2. Spectral fit results with non-relativistic model `tbabs(diskbb+gaussian+nthComp)`^a. From left to right, are (1) name of observation (2) hydrogen column density in units of $\times 10^{22}$ atoms cm^{-2} ; (3) inner disk temperature in units of keV; (4) normalization constant for `diskbb` in units of $\times 10^4$; (5) photon power-law index; (6) electron temperature in units of keV; (7) seed photon temperature in units of keV; (8) normalization constant for `nthComp`; (9) unabsorbed flux, calculated in 0.1 – 100.0 keV energy range, in units of $\times 10^{-8}$ ergs $\text{cm}^{-2} \text{s}^{-1}$; (10) χ^2_{red} (χ^2/dof ; dof \equiv degree of freedom) resulting from fit. See text for details.

Obs	N_H	kT_{in}	N_{disk}	Γ	kT_e	kT_{bb}	$N_{nthComp}$	Flux	$\chi^2_{red}(\chi^2/\text{dof})$
Obs A	0.75 ± 0.01	-	-	1.59 ± 0.01	$86.94^{+81.89}_{-21.91}$	0.1 (fixed)	0.84 ± 0.01	2.56	1.33(848.72/638)
Obs B	0.54 ± 0.01	-	-	1.59 ± 0.01	$46.99^{+1.71}_{-3.31}$	0.1 (fixed)	1.15 ± 0.01	3.49	1.18(739.52/624)
Obs C	$0.73^{+0.03}_{-0.02}$	0.29 ± 0.01	$18.18^{+3.61}_{-2.76}$	1.91 ± 0.01	120 (fixed)	$0.16^{+0.12}_{-0.06}$	$2.64^{+0.18}_{-1.02}$	6.03	1.01(627.13/620)
Obs D	$0.73^{+0.04}_{-0.03}$	0.31 ± 0.01	$12.66^{+2.52}_{-1.80}$	1.86 ± 0.01	80 (fixed)	$0.17^{+0.20}_{-0.04}$	$2.22^{+0.14}_{-0.70}$	6.23	1.19(750.44/627)
Obs E	0.67 ± 0.01	0.43 ± 0.01	$2.94^{+0.28}_{-0.26}$	2.28 ± 0.01	$43.99^{+13.27}_{-7.76}$	0.16 ± 0.01	$7.33^{+0.30}_{-0.33}$	6.35	1.48(927.65/624)
Obs F	0.7 (fixed)	0.43 ± 0.01	$3.26^{+0.21}_{-0.19}$	2.66 ± 0.01	300 (fixed)	0.13 ± 0.01	$15.46^{+0.34}_{-0.42}$	7.55	1.56(990.00/633)
Obs G	0.69 ± 0.01	0.46 ± 0.01	3.45 ± 0.20	3.15 ± 0.03	300 (fixed)	0.15 ± 0.01	$10.92^{+0.60}_{-0.58}$	7.17	1.78(946.08/530)
Obs H	0.7 (fixed)	0.40 ± 0.01	$4.94^{+0.28}_{-0.27}$	2.64 ± 0.01	150 (fixed)	0.13 ± 0.01	$15.34^{+0.21}_{-0.25}$	9.15	1.67(1021.92/611)
Obs I	0.69 ± 0.01	0.45 ± 0.01	$4.43^{+0.13}_{-0.15}$	2.57 ± 0.01	300 (fixed)	0.13 ± 0.01	$4.95^{+0.16}_{-0.20}$	6.26	1.80(1072.92/594)

^a Note: The model is multiplied with `smedge` to represent the absorption feature. The component consists of a threshold energy (E_c), maximum absorption factor at threshold (f), index for photo-electric cross-section (α) and smearing width (w). The parameters E_c , f , α and w are found to be varying in range of 7.3-8.0 keV, 0.5 to 3.6, -1.3 to -2.9 and 2.4 to 9.6 keV, respectively.

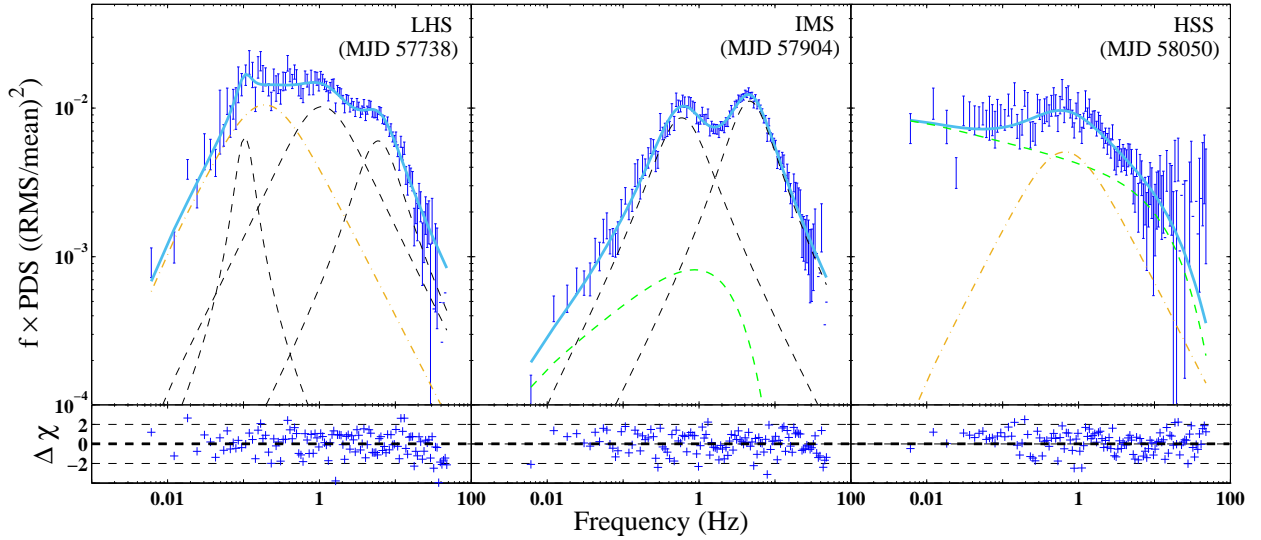


Figure 4. Model fitted PDS (solid cyan line) in frequency 0.006 – 50.0 Hz of low-hard state (left), intermediate state (middle) and high-soft state (right) of Cygnus X-1 for observation B, D and G unfolded against the models. The fits are performed for the energy range from 3.0–50.0 keV using *LAXPC* data. The fit model includes multiple Lorentzians (black and yellow dashed line) for narrow or broad profiles plus cut-off power-law component (dashed green line). Zero centered Lorentzians represent broadband limited noise (BLN) shown in yellow dashed line. Bottom panels show the corresponding residuals in units of σ . See text for details.

Table 3. The best-fit parameters results from fitting models to PDS. From left to right, are (1) name of observation; (2) width of zero centered Lorentzians representing BLN; (3)-(8) frequencies and corresponding widths of Lorentzians; (9) index of cut-off power-law; (10) fractional RMS of BLN component in percentage; (11) total fractional RMS; (12) fractional flux variability; (13) χ^2_{red} (χ^2/dof ; dof \equiv degree of freedom) resulting from fit. See text for details.

Obs	σ_1 (FWHM)	ν_2 (Hz)	σ_2 (FWHM)	ν_3 (Hz)	σ_3 (FWHM)	ν_4 (Hz)	σ_4 (FWHM)	α	RMS _{BLN} (%)	RMS _{total} (%)	F _{var} (%)	$\chi^2_{red}(\chi^2/\text{dof})$
Obs A	$0.32^{+0.04}_{-0.03}$	$0.60^{+0.13}_{-0.17}$	2.04 ± 0.21	4.44 ± 0.36	$7.27^{+0.31}_{-0.33}$	0.07 ± 0.01	$0.010^{+0.008}_{-0.007}$	-	20.64	28.16	37.7	1.29(144.09/111)
Obs B	$0.37^{+0.07}_{-0.03}$	$0.32^{+0.21}_{-0.22}$	$2.03^{+0.21}_{-0.14}$	$4.54^{+0.36}_{-0.42}$	$7.70^{+0.36}_{-0.37}$	0.1 (fixed)	$0.06^{+0.007}_{-0.02}$	-	17.87	27.60	33.5	1.66(184.63/111)
Obs C	-	$0.42^{+0.06}_{-0.05}$	$1.45^{+0.07}_{-0.10}$	4.6 ± 0.08	$5.80^{+0.16}_{-0.15}$	-	-	$0.68^{+0.22}_{-0.21}$	-	20.11	38.2	1.54(176.19/114)
Obs D	-	0.38 ± 0.03	0.90 ± 0.06	3.44 ± 0.09	6.21 ± 0.14	-	-	$0.56^{+0.21}_{-0.08}$	-	20.47	33.8	1.28(146.40/114)
Obs E	-	-	-	-	-	-	-	0.97 ± 0.01	-	25.94	28.3	1.58(188.30/119)
Obs F	$0.39^{+0.06}_{-0.05}$	-	-	-	-	-	-	0.96 ± 0.02	13.47	28.43	27.7	1.72(201.70/117)
Obs G	1.32 ± 0.13	-	-	-	-	-	-	1.12 ± 0.04	12.59	24.99	20.1	1.32(155.07/117)
Obs H	$0.54^{+0.07}_{-0.06}$	-	-	-	-	-	-	0.98 ± 0.01	10.66	27.94	21.1	1.47(172.45/117)

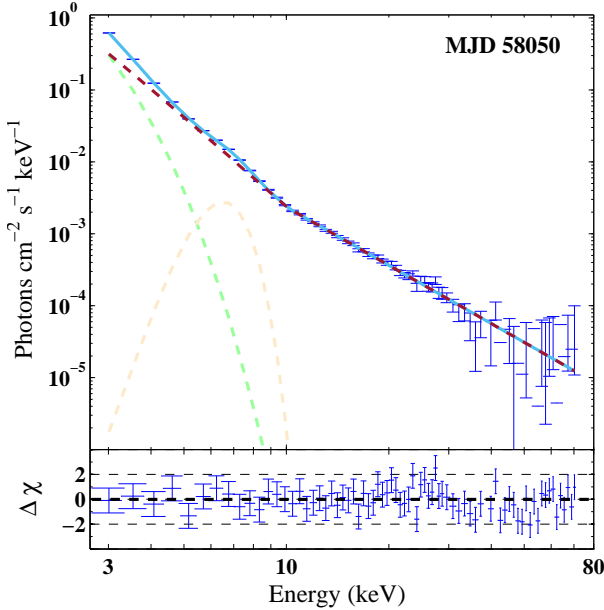


Figure 5. The softest spectrum of Cygnus X-1, from observation on Oct 24, 2017 (MJD 58050), fitted with an absorbed disk (`diskbb`) plus broken power-law (`bknpower`). Overall fit is shown with solid cyan line. The disk, broken power-law and Gaussian profile of Iron line is shown with green, brown and orange dashed line, respectively. The lower panel shows the fit residual in units of σ . The scheme prescribed by Wilms et al. (2006) is followed to estimate the low energy spectral index Γ_1 (~ 4.13). See §5 for details.

5 THE CONTINUUM-FITTING AND THE SOFTEST STATE OF CYGNUS X-1

5.1 The Softest Nature of Cygnus X-1: *AstroSat* and Previous Observations

Cygnus X-1, although persistently remains in hard state but occasionally it transits to extreme soft states. The spectral analysis described in §3 indicates that *AstroSat* observation of Cygnus X-1 on Oct 24, 2017 (Obs G) is very distinctive in terms of spectral softness and the spectral characteristics, which exhibits an extremely soft nature. In order to carry out a comparative study of this soft nature of the source with previously reported as the softest state by Kawano et al. (2017) from *Suzaku* observations on May 07, 2013, an in-depth analysis of the *AstroSat* data is performed.

Firstly, *MAXI*-HR for Oct 24, 2017 (MJD 58050) is obtained and it is compared with the same for May 07, 2013 (MJD 56419). We find that *MAXI*-HR drops to ~ 0.229 during *AstroSat* observation, while the same corresponding to *Suzaku* observations is at higher value of ~ 0.238 (see Figure 1). The lower *MAXI*-HR value is an indicative of more soft energy photon flux relative to that of in hard energy. Secondly, *LAXPC* lightcurve is also examined and we obtain the hardness ratio (hereafter *LAXPC*-HR) of photon counts in energy range 10.0 – 50.0 keV to 3.0 – 10.0 keV. We choose these energy ranges as it is noted in the spectral analysis (§3) that disk component extends upto ~ 10 keV whereas the photon flux in 10.0 – 50.0 is attributed to Comptonisation component. Hence, the *LAXPC*-HR reflects

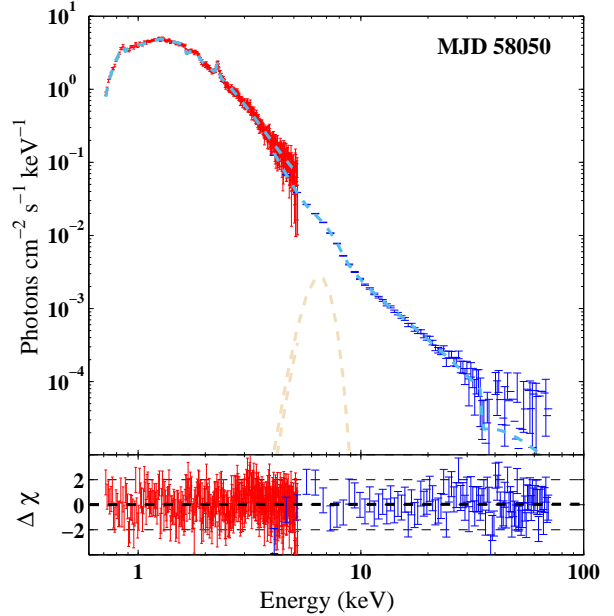


Figure 6. Spectrum of Cygnus X-1, observed on Oct 24, 2017 (MJD 58050), fitted with relativistic model. The model comprises of an absorbed *kerrbb* convoluted with *simpl*. Cyan dashed line shows the total model. Gaussian profile of Iron line is shown with orange dashed line. Bottom panels show the corresponding residuals in units of σ . See §5.2 for details.

variation of the relative contributions of disk component and Comptonised emission component in total spectrum with time. We notice a time interval where the *LAXPC*-HR remains about a minimum value of ~ 0.27 . Subsequently, *SXT* and *LAXPC* spectra from Obs G data are extracted for this time interval only. This extracted spectrum is further used to compare the spectral softness of the source with that of described in Kawano et al. (2017). We follow the same method adopted by Kawano et al. (2017) and fit an absorbed disk plus broken power-law model over *LAXPC* spectrum (3.0–70.0 keV). The method, defining the spectral nature in Cygnus X-1, is prescribed by Wilms et al. (2006) and Grinberg et al. (2014), which is based on low energy index of broken power-law. The low energy photon index Γ_1 suggests the disk dominance over high energy tail. We estimate the low energy photon index $\Gamma_1 = 4.13^{+0.06}_{-0.08}$, which is even higher than that of the softest state reported by Kawano et al. (2017) as $\Gamma_1 \sim 4.0$. The model fitted *LAXPC* spectrum is shown in Figure 5.

Combining the results from these two methods, it is evident that Cygnus X-1 during *AstroSat* observation on MJD 58050 (Obs G) exhibits a minimum value of *MAXI*-HR and a steeper of low energy photon index (Γ_1) than those of during *Suzaku* observations. The two findings corroborate the highest contribution of soft disk component in total spectrum ever observed from the source.

5.2 Constraining the Spin of Cygnus X-1

In previous sections (§3.1 and §5.1), it is shown that the source exhibits an extreme soft state during *AstroSat* obser-

Table 4. Spectral fit results with relativistic model `tbabs*(simpl@kerrbb+gaussian)`. Parameters are (top to bottom) (1) hydrogen column density in units of $\times 10^{22}$ atoms cm^{-2} ; (2) photon power-law index; (3) scattering fraction in percentage; (4) spin parameter; (5) mass accretion rate in units of $\times 10^{18}$ gm s^{-1} ; (6) mass of black hole in units of M_{\odot} ; (7) distance to Cygnus X-1 in units of kpc; (8) inclination of binary plane in degrees; (9) spectral hardening factor. Orbit number provided for Obs G and I are the spacecraft orbit numbers.

Components	Parameter	Obs G		Obs I
		Orbit 11212	Orbit 11215	Orbit 15548
<i>tbabs</i>	N_H	0.67 ± 0.01	0.66 ± 0.02	$0.68^{+0.02}_{-0.01}$
<i>simpl</i>	Γ	2.98 ± 0.02	2.21 ± 0.03	2.61 ± 0.01
	f_{sc}	$10.56^{+0.22}_{-0.31}$	5.56 ± 0.01	$11.08^{+0.32}_{-0.21}$
<i>kerrbb</i>	a_*	$0.9998^{+0.0000}_{-0.0015}$	$0.9999^{+0.0000}_{-0.0121}$	$0.9998^{+0.0000}_{-0.0155}$
	\dot{M}	$0.14^{+0.02}_{-0.01}$	0.12 ± 0.01	0.11 ± 0.02
	M_{BH}	21.2 (fixed)	21.2 (fixed)	21.2 (fixed)
	D_{BH}	2.22 (fixed)	2.22 (fixed)	2.22 (fixed)
	i	27.5 (fixed)	27.5 (fixed)	27.5 (fixed)
	f	$1.73^{+0.01}_{-0.01}$	$1.74^{+0.01}_{-0.02}$	$1.82^{+0.01}_{-0.02}$
$\chi^2_{\text{red}} (\chi^2/\text{dof})$		1.32 (712.8/540)	1.31 (719.6/546)	1.42 (732.71/516)

vations (Obs G). Further, the continuum-fitting method is employed and spectrum of HSS is modelled with relativistic model to estimate the spin. For relativistic modeling of spectrum, we follow Gou et al. (2014) and Kawano et al. (2017) and use `constant * tbabs(simpl @ kerrbb + gaussian)` model to fit the spectrum. `simpl` is a Comptonising convolution model, which produces power-law distribution in higher energies using soft seed photons from accretion disk independently irrespective of any shape or location of Comptonising medium (Steiner et al. 2009a). The `simpl` estimates two parameters, f_{sc} and Γ . f_{sc} gives the fraction of seed photons up-scattered to power-law tail while Γ estimates the steepness of this tail. `kerrbb` is a relativistic thin accretion disk model which includes self-irradiation and limb-darkening effects (Li et al. 2005). We switch off limb-darkening and apply zero torque condition at the inner boundary of the disk. Moreover, model is provided with updated measurements of distance to source (D), mass of the black hole (M_{BH}) in the binary system and inclination of the binary plane (i) as mentioned in §1 and thus the normalization is fixed to unity. The other two parameters, namely accretion rate (\dot{M}) and spectral hardening factor (f) are allowed to vary freely. The `gaussian` component is added to model the Iron line profile. Further, in order to achieve acceptable fit results, we correct for instrument features at 1.8 and 2.24 keV arising from SXT. Also, a broad absorption dip present at ~ 8 keV is modelled with `smedge`. The overall fit results in χ^2_{red} of $712.8/540 = 1.32$. The model fitted spectrum is shown in Figure 6. \dot{M} is estimated as $\sim 0.14 \times 10^{18}$ g s^{-1} . Spectral hardening factor (f) is determined as 1.73 ± 0.01 , which is in good agreement with values suggested for stellar mass black holes (Shimura & Takahara 1995). The scattering fraction f_{sc} comes to be $10.56^{+0.22}_{-0.31}\%$, which implies that the data is of good quality and it well satisfies the criterion for continuum-fitting method (Steiner et al. 2009b). The fit gives the power-law index (Γ) of 2.98 ± 0.02 , which is comparable with the estimate of $\Gamma = 2.93^{+0.11}_{-0.05}$ by Kawano et al. (2017). This again indicates that during *AstroSat* observation Cygnus X-1 shows the weakest Comptonisation tail. The best fit gives an extreme value of the spin parameter as $a_* = 0.9998^{+0.0000}_{-0.0015}$, which is very close to the hard limit of `kerrbb` model. In order to estimate the errors on spin pa-

rameter we perform Monte Carlo (MC) simulations, which is discussed later in the section. Additionally, the similar fit procedure is applied to two more observations (Obs G, Orbit no. 11215 and Obs I) where spectra are suitable for spin estimations. Although these spectra have less steeper Γ than that of Obs G (Orbit no. 11212), however, the fits give acceptable f_{sc} values, which further made them reliable for spin estimation. The spectral fit parameters are provided in Table 4.

Further, to estimate the uncertainties in spin parameter values, obtained from each spectra, we perform MC simulations and generate 20000 sets of binary system parameters (M_{BH} , i and D), as previous spin estimation works suggest that uncertainties in these three input parameters dominate over the errors resulting from `kerrbb` model (Gou et al. 2011; McClintock et al. 2014; Zhao et al. 2021). The sets are generated assuming independent Gaussian-distributions for each parameter. Subsequently, we calculate the look-up table of hardening factor (f), corresponding to each parameter set and then fit the spectra to determine spin parameters. This gives 20000 values of spin parameters per spectrum. We repeat this procedure on all three observations and finally, obtain respective histograms of a_* , which are shown in Figure 7. We consider the lowest spin parameter value of all the three observations, for the final estimation of spin as $a_* > 0.9981$ at 3σ confidence level. We also calculate the spin parameter with a summed up histogram of all the observations, which also results into the similar value with 3σ confidence. The lower limits for 2σ and 1σ are 0.9988 and 0.9995, respectively. Similar lower limits for individual spectrum are marked in Figure 7.

6 DISCUSSION AND CONCLUSION

AstroSat made several co-ordinated observations on Cygnus X-1, starting from 2016 to 2020. Initially in the year 2016 the source is in low-hard state. In March, 2017, the source starts to show signature of transition from the persistent low-hard state. The simultaneous and continuous monitoring by *MAXI* also exhibits a clear transition with a decreasing spectral hardness ratio value from its mean value of ~ 0.8 (see Figure 1). The hardness ratio consistently keeps

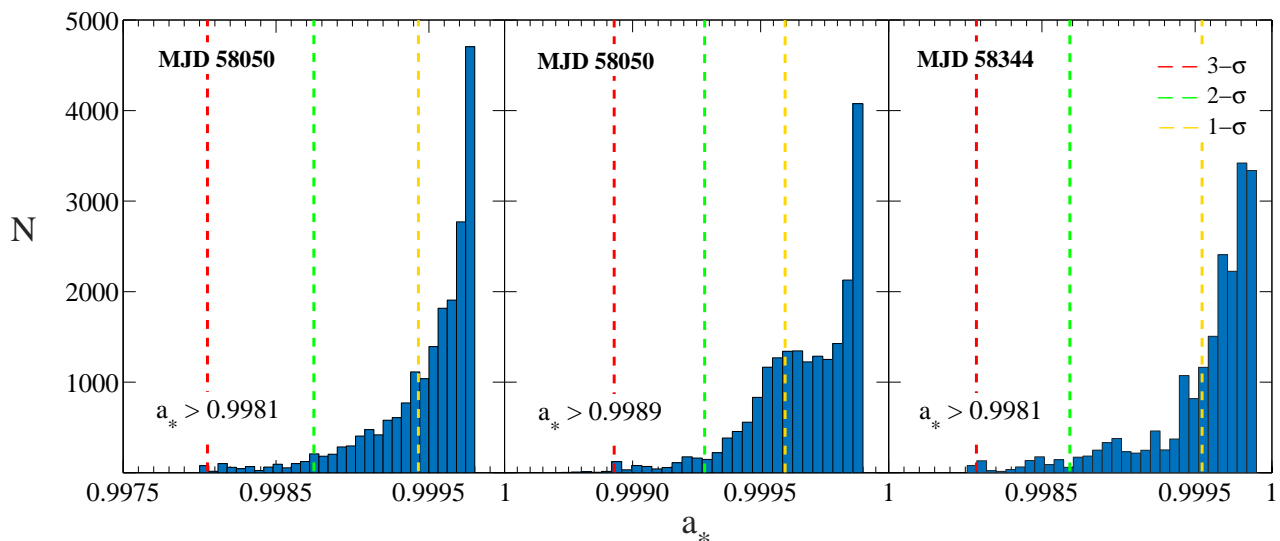


Figure 7. The histograms of spin parameter (a_*) resulting from Monte Carlo simulations with 20000 sets of parameters, containing mass of the blackhole (M_{BH}), inclination of the binary (i) and distance to the source (D), per spectrum. The three vertical dashed lines, from left to right in each panel, mark the error confidence of 3σ (99.7%, red), 2σ (95.4%, green) and 1σ (68.3%, yellow). The corresponding 3σ confidence lower limits of a_* is also given in each panel. The left, middle and right histogram panels are obtained from observation G (orbit no. 11212), G (orbit no, 11215) and I, respectively. See text for details.

decreasing till Oct, 2017, while the source passes through intermediate state and attains a high-soft state. Cygnus X-1, in a period of about 7 months starting from March, 2017 till Sept, 2017, completely transits to a high-soft state. The source remains in soft state for about two months. We observe that the hardness ratio of the source decreases to the lowest value of ~ 0.229 . From Nov, 2017 onwards, it is observed that there is increase in hardness ratio which marks the transition back to the low-hard state. Subsequently, the source shows flickering sequence of transitions from hard to soft states and vice versa (see Figure 1). *AstroSat* observations sample the transition of Cygnus X-1 in year 2017 from LHS to HSS via IMS (see Figure 1 and Table 1). We make use of data from *SXT* and *LAXPC* X-ray instruments onboard *AstroSat* and study the evolution of spectral and temporal properties of the source during the transition including hard and extreme soft states.

SXT & *LAXPC* combined spectra are modelled in 0.5–70.0 keV energy range. Spectra from LHS of Cygnus X-1 are modelled with absorbed non-thermal Comptonisation model (*nthComp*) with out any signature of thermal component in this state. Spectral indices (Γ) of 1.59 ± 0.01 are found to be in good agreement with usual LHS spectral index of Cygnus X-1 (Grinberg et al. 2014) as well as with other BH-XRBs (GX 339–4 Nandi et al. (2012), IGR 17091–3624 Radhika et al. (2018), 4U 1630-472 Baby et al. (2020)). In subsequent IMS, we find that spectral indices (Γ) are steeper with values ranging in 1.86–2.28. Along with that there is an indication of thermal disk emission component (*diskbb*) with inner disk temperature (kT_{in}) in range of 0.29–0.43 keV. Further, during IMS, we note that with increase of spectral index, the inner disk temperature increases as well while the normalisation of disk component decreases. This could suggest that the disk approaches towards the central object. Subsequent observations in Oct, 2017 show that source is in HSS and

the spectral indices are even steeper with values lying in 2.5–3.15. During HSS, from Obs G on Oct 24, 2017 (MJD 58050), we find that spectral index of source is the steepest with $\Gamma = 3.15 \pm 0.03$ along with an inner disk temperature (kT_{in}) of 0.46 ± 0.01 keV. Similar steep spectral nature and inner disk temperature, during HSS of other BH-XRBs have been reported previously. For example, findings from the HSS of GX 339–4 by Nandi et al. (2012) show an inner disk temperature and photon index of ~ 0.7 keV and ~ 3.5 respectively. Radhika et al. (2018) has shown for IGR 17091–3624 that the inner disk temperature reaches upto 1.3 keV in HSS. Further, we observe that the inner disk temperature increases consistently with increase in spectral index from LHS to HSS, which is shown in Figure 8. Along with this, we note that the fractional disk flux contributions in net spectra vary in 33%–45% during IMS to HSS. The maximum fractional disk contribution of $\sim 45\%$ is observed in Obs G of HSS. It is to be noted that the model with combination of *diskbb* and *nthComp* results in slightly higher values of χ^2_{red} (> 1.5), indicating further investigation to improve modelling of the HSS spectra. Although, for uniformity and comparative study of spectral parameters we use the same model for all the states. Further, based on the inner disk temperature (kT_{in}) and photon index (Γ) we classify the observed spectra into three states, namely, LHS, IMS and HSS (see §3.1 and Figure 8). We also estimate the unabsorbed flux 0.1–100.0 keV energy range for all states (see Figure 8) and compare it with Eddington luminosity. We notice that luminosity of the source varies from 0.3% to $\sim 1.4\%$ of Eddington luminosity (L_{edd} ⁶) of Cygnus X-1. The luminosities during different states of the source are in good agreements with previous findings by Gou et al. (2011); Yamada et al. (2013); Gou et al. (2014);

⁶ For Cygnus X-1 $L_{\text{edd}} \approx 2.8 \times 10^{39}$ ergs s^{-1}

Tomsick et al. (2014); Walton et al. (2016); Basak et al. (2017); Tomsick et al. (2018).

Also, we examine the power density spectra (PDS) of Cygnus X-1 simultaneous to spectral analysis. PDS of LHS & IMS show multiple broad **lorentzians** features along with band limited noise. In soft states of the source, we observe that broad features are absent and PDS show a steep cut-off power-law with index of ~ 1 and again a band limited noise is present. The temporal features of Cygnus X-1 are in good agreement with previous studies by (Pottschmidt et al. 2003; Axelsson et al. 2005; Misra et al. 2017). Non-detection of QPO like features in HSS of Cygnus X-1 is quite common as the featureless PDS are observed in other BH-XRBs too (see Radhika & Nandi (2014); Nandi et al. (2018) for XTE J1859 + 226, Radhika et al. (2016) for V404 Cyg, Belloni et al. (2005); Nandi et al. (2012) for GX 339 – 4).

Furthermore, we highlight the results of Obs G of HSS as it's PDS shows the steepest power-law index with a value of 1.12 ± 0.04 . Also the band limited noise show the largest FWHM of 1.32 Hz. We also calculate the flux variability (F_{var}) in lightcurves during all the observations and note an anti-correlation with corresponding RMS calculated from PDS modelling (see Figure 8). The variation of RMS is also noticed with spectral index (Γ), which agrees to that of Grinberg et al. (2014). During HSS, an RMS value of $\sim 25\%$ is observed which is comparable to that of in LHS. Display of such high RMS is a typical characteristics of Cygnus X-1 (Grinberg et al. 2014) and unlike the general nature of BH-XRBs (Belloni 2010), RMS does not drop to very low values. For example, GX 339 – 4 and IGR 17091 – 3624 exhibit a low RMS of $\sim 3\%$ in HSS (Nandi et al. 2012; Radhika et al. 2018). Recently, Sreehari et al. (2020) show in case of HSS of GRS 1915 + 105, a total RMS less than 2%.

Moreover, we find that the high-soft state of Cygnus X-1 is unprecedented and *AstroSat* on Oct 24, 2017 (MJD 58050) observed the source in an extremely soft state. We compare the soft nature of source during *AstroSat* era with previously reported the softest state of Cygnus X-1 by Kawano et al. (2017) with *Suzaku* observations on May 07, 2013 (MJD 56419). We note the following two criteria for the comparison. Firstly, the hardness ratio obtained from *MAXI* on MJD 58050 with the lower value of ~ 0.229 indicates the *AstroSat* observations are softer than that of during *Suzaku* observations. Secondly, we adopt similar method of modelling spectra with broken power law in range 3.0–70.0 keV as adopted by Kawano et al. (2017). We find that the low energy photon index (Γ_1) of broken power-law is even steeper with a value of $4.13^{+0.06}_{-0.08}$ than that of estimated by Kawano et al. (2017) as ~ 4.0 , which confirms the largest contribution of disk component in net spectrum ever recorded. Hence, in this work, we confirm the softest state of Cygnus X-1 ever observed. It is to be noted that Cygnus X-1 occasionally enters in a high-soft state and it has never reached 'canonical' soft state.

Further, we make use of the high quality data from *AstroSat* observations of the softest state of the source to constrain the spin of black hole as the spectra are dominated with disk component and are suitable for continuum-fitting (CF) method. We fit the spectra with **kerrbb** convoluted with **simpl** in order to constrain the spin parameter (a_*) of the black hole. Furthermore, we perform MC simulations to estimate the uncertainty in a_* , combining the errors in the

binary system parameters, M_{BH} , i and D . We report the spin parameter of Cygnus X-1 as $a_* > 0.9981$ at 3σ (99.7%) confidence level, which suggests an extreme spin of the black hole in Cygnus X-1.

We compare the spin measurement results with those obtained by Zhao et al. (2021) recently, as $a_* > 0.9985$ (3σ). The spin estimation in this work is in good agreement with their results. Also, Zhao et al. (2020) applied CF method on large set of spectra obtained from *HXMT* and estimated lower limit of the spin parameter as $a_* > 0.967$ (3σ) using revised values of M_{BH} , i and D .

Previously, Gou et al. (2014) employed CF method and estimated $a_* > 0.983$ at a confidence level of 3σ (99.7%). Kawano et al. (2017) determined $a_* = 0.95 \pm 0.01$ with similar method using data from *Suzaku*. Spin estimation by Tomsick et al. (2014) with Fe- K_α line fitting method using *Suzaku* and *NuSTAR* data resulted as $a_* = 0.9882 \pm 0.0009$ (90% confidence level).

Focusing on other parameters of best-fit, we state that the scattering fraction (f_{sc}) comes to be $10.56^{+0.22}_{-0.31}\%$. Furthermore, we observe from spectral fit that the luminosity of the disk component is consistent in HSS with $L/L_{Edd} \sim 1.4\%$. These parameters satisfy the criterion for application of continuum-fitting method to produce reliable results as stated in §1.

Moreover, these results of continuum-method are based on Novikov-Thorne model. The model assumes a zero torque which introduces uncertainties in spin estimation. These uncertainties are very small as a_* tends to unity. Also, the model originated errors are much smaller than the errors in measurements of M_{BH} , i and D , which is important in case of thin disks. Another possible error can be from pile-up in *SXT* detector during high flux soft states. In order to estimate pile-up, we fit only *LAXPC* spectra to find out any spectral hardening from pile-up. It is observed that photon index varies by less than 2%, which is expected due to channel difference in two detectors. Hence, we conclude that spin estimations obtained are fairly reliable.

In order to summarize, in this paper, we present an in-depth spectral and timing analysis results obtained from *AstroSat* observations of Cygnus X-1 during transition from hard state to soft state via intermediate states. Moreover, we confirm the detection of the 'softest' nature ever observed from the source with *AstroSat*. We make use of the high quality spectral data of the softest state to constrain the spin parameter of the black hole. Finally, considering the present estimates of spin and mass, we conclude that Cygnus X-1 is a maximally rotating, massive black hole binary source. This compact nature echoes to that of the enigmatic galactic black hole source GRS 1915 + 105, which represents a standard template for BH-XRBs (Sreehari et al. 2020).

ACKNOWLEDGEMENTS

We are thankful to the anonymous referee for giving valuable suggestions to improve on spin estimation results. We also thank Sreehari from Indian Institute of Astrophysics (IIA) for his help in modelling. This publication uses the data from the *AstroSat* mission of the Indian Space Research Organisation (ISRO), archived at the Indian Space Science Data Centre (ISSDC). This work has used the data from the

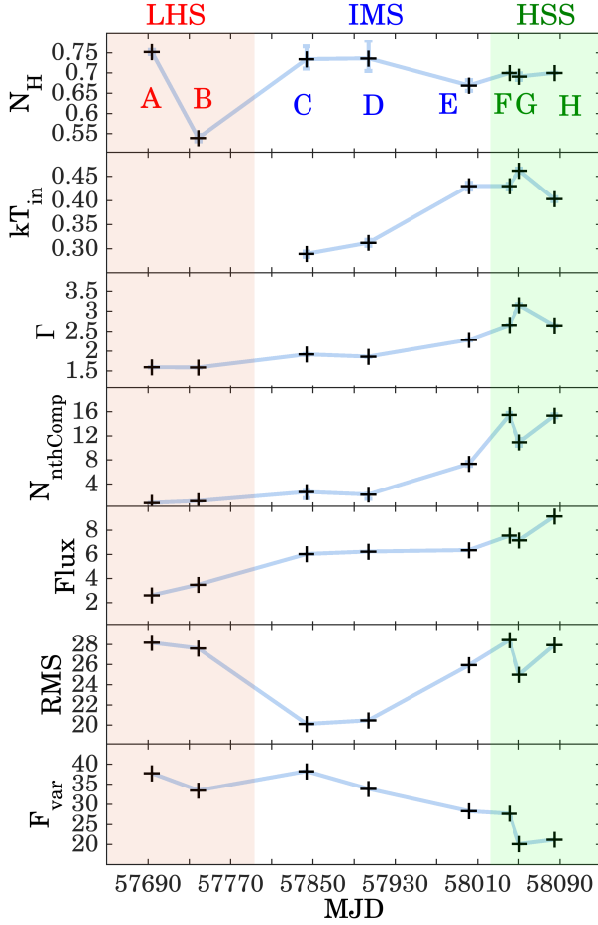


Figure 8. The evolution of spectral and timing parameters of Cygnus X-1, during transition from LHS to HSS via IMS. The parameters are (top to bottom) hydrogen column density (N_H) in units of $\times 10^{22}$ atoms cm^{-2} , inner disk temperature (kT_m) in units of keV, photon index (Γ), normalization constant of `nthComp`, unabsorbed flux, calculated in 0.1 – 100.0 keV energy range, in units of $\times 10^{-8}$ ergs cm^{-2} s^{-1} , total fractional RMS of PDS in percent, fractional flux variability in percentage (see text for details). Observations from A to H are marked and shown in top panel. Red shaded region represents LHS, blue is IMS and green shows HSS. For Obs A & B inner disk temperature is not shown as the disk component is not required to model the LHS spectra.

Soft X-ray Telescope (*SXT*) developed at TIFR, Mumbai, and the *SXT* POC at TIFR is thanked for verifying and releasing the data and providing the necessary software tools. This work has also used the data from the *LAXPC* Instruments developed at TIFR, Mumbai, and the *LAXPC* POC at TIFR is thanked for verifying and releasing the data. We thank the *AstroSat* Science Support Cell hosted by IUCAA and TIFR for providing the *LaxpcSoft* software which we used for *LAXPC* data analysis. Authors thank GH, SAG; DD, PDMSA and Director, URSC for encouragement and continuous support to carry out this research.

DATA AVAILABILITY STATEMENT

Data used for this work are available at *AstroSat*-ISSDC website

(http://astrobrowse.issdc.gov.in/astro_archive/archive), and *MAXI* website (<http://maxi.riken.jp/top/index.html>).

REFERENCES

- Abramowicz M. A., Kluźniak W., 2001, *A&A*, **374**, L19
 Agrawal P. C., 2006, *Advances in Space Research*, **38**, 2989
 Agrawal V. K., Nandi A., 2020, *MNRAS*, **497**, 3726
 Agrawal P. C., et al., 2017, *Journal of Astrophysics and Astronomy*, **38**, 30
 Agrawal V. K., Nandi A., Girish V., Ramadevi M. C., 2018, *MNRAS*, **477**, 5437
 Agrawal V. K., Nandi A., Ramadevi M. C., 2020, *Ap&SS*, **365**, 41
 Antia H. M., et al., 2017, *ApJS*, **231**, 10
 Antia H. M., et al., 2021, arXiv e-prints, p. arXiv:2101.07514
 Axelsson M., Borgonovo L., Larsson S., 2005, *A&A*, **438**, 999
 Baby B. E., Agrawal V. K., Ramadevi M. C., Katoch T., Antia H. M., Mandal S., Nandi A., 2020, *MNRAS*, **497**, 1197
 Bardeen J. M., Press W. H., Teukolsky S. A., 1972, *ApJ*, **178**, 347
 Basak R., Zdziarski A. A., Parker M., Islam N., 2017, *MNRAS*, **472**, 4220
 Belloni T. M., 2010, States and Transitions in Black Hole Binaries. p. 53, doi:10.1007/978-3-540-76937-8_3
 Belloni T., Hasinger G., 1990, *A&A*, **227**, L33
 Belloni T., van der Klis M., Lewin W. H. G., van Paradijs J., Dotani T., Mitsuda K., Miyamoto S., 1997, *A&A*, **322**, 857
 Belloni T., Homan J., Casella P., van der Klis M., Nespoli E., Lewin W. H. G., Miller J. M., Méndez M., 2005, *A&A*, **440**, 207
 Bolton C. T., 1972, *Nature Physical Science*, **240**, 124
 Chakrabarti S., Titarchuk L. G., 1995, *ApJ*, **455**, 623
 Churazov E., Gilfanov M., Revnivtsev M., 2001, *MNRAS*, **321**, 759
 Dihingia I. K., Das S., Nandi A., 2019, *MNRAS*, **484**, 3209
 Dovčiak M., Muleri F., Goosmann R. W., Karas V., Matt G., 2008, *MNRAS*, **391**, 32
 Foreman-Mackey D., Hogg D. W., Lang D., Goodman J., 2013, *PASP*, **125**, 306
 Gierliński M., Zdziarski A. A., Poutanen J., Coppi P. S., Ebisawa K., Johnson W. N., 1999, *MNRAS*, **309**, 496
 Goodman J., Weare J., 2010, *Communications in Applied Mathematics and Computational Science*, **5**, 65
 Gou L., et al., 2009, *ApJ*, **701**, 1076
 Gou L., et al., 2011, *ApJ*, **742**, 85
 Gou L., et al., 2014, *ApJ*, **790**, 29
 Grinberg V., et al., 2014, *A&A*, **565**, A1
 Homan J., Belloni T., 2005, *Ap&SS*, **300**, 107
 Homan J., Wijnands R., van der Klis M., Belloni T., van Paradijs J., Klein-Wolt M., Fender R., Méndez M., 2001, *ApJS*, **132**, 377
 Kawano T., Done C., Yamada S., Takahashi H., Axelsson M., Fukazawa Y., 2017, *PASJ*, **69**, 36
 Li L.-X., Zimmerman E. R., Narayan R., McClintock J. E., 2005, *ApJS*, **157**, 335
 Ling J. C., Mahoney W. A., Wheaton W. A., Jacobson A. S., Kaluzienski L., 1983, *ApJ*, **275**, 307
 Mandal S., Chakrabarti S. K., 2007, *Ap&SS*, **309**, 305
 McClintock J. E., Shafee R., Narayan R., Remillard R. A., Davis S. W., Li L.-X., 2006, *ApJ*, **652**, 518
 McClintock J. E., Narayan R., Steiner J. F., 2014, *Space Sci. Rev.*, **183**, 295
 Mihara T., et al., 2011, *PASJ*, **63**, S623
 Miller-Jones J. C. A., et al., 2021, *Science*, **371**, 1046
 Misra R., et al., 2017, *ApJ*, **835**, 195
 Mitsuda K., et al., 1984, *PASJ*, **36**, 741

Miyamoto S., Kitamoto S., Iga S., Negoro H., Terada K., 1992, *ApJ*, **391**, L21

Nandi A., Debnath D., Mandal S., Chakrabarti S. K., 2012, *A&A*, **542**, A56

Nandi A., et al., 2018, *Ap&SS*, **363**, 90

Novikov I. D., Thorne K. S., 1973, in *Black Holes (Les Astres Occlus)*. pp 343–450

Orosz J. A., McClintock J. E., Aufdenberg J. P., Remillard R. A., Reid M. J., Narayan R., Gou L., 2011, *ApJ*, **742**, 84

Parker M. L., et al., 2015, *ApJ*, **808**, 9

Pottschmidt K., et al., 2003, *A&A*, **407**, 1039

Radhika D., Nandi A., 2014, *Advances in Space Research*, **54**, 1678

Radhika D., Nandi A., Agrawal V. K., Seetha S., 2016, *MNRAS*, **460**, 4403

Radhika D., Sreehari H., Nandi A., Iyer N., Mandal S., 2018, *Ap&SS*, **363**, 189

Rao A. R., Singh K. P., Bhattacharya D., 2016, arXiv e-prints, p. arXiv:1608.06051

Reid M. J., McClintock J. E., Narayan R., Gou L., Remillard R. A., Orosz J. A., 2011, *ApJ*, **742**, 83

Remillard R. A., McClintock J. E., 2006, *ARA&A*, **44**, 49

Reynolds C. S., 2014, *Space Sci. Rev.*, **183**, 277

Schnittman J. D., Krolik J. H., 2009, *ApJ*, **701**, 1175

Shakura N. I., Sunyaev R. A., 1973, *A&A*, **500**, 33

Shimura T., Takahara F., 1995, *ApJ*, **445**, 780

Singh K. P., et al., 2014, ASTROSAT mission. p. 91441S, doi:10.1117/12.2062667

Singh K. P., et al., 2016, In-orbit performance of SXT aboard AstroSat. p. 99051E, doi:10.1117/12.2235309

Singh K. P., et al., 2017, *Journal of Astrophysics and Astronomy*, **38**, 29

Sreehari H., Ravishankar B. T., Iyer N., Agrawal V. K., Katoch T. B., Mandal S., Nandi A., 2019, *MNRAS*, **487**, 928

Sreehari H., Nandi A., Das S., Agrawal V. K., Mandal S., Ramadevi M. C., Katoch T., 2020, arXiv e-prints, p. arXiv:2010.03782

Steiner J. F., Narayan R., McClintock J. E., Ebisawa K., 2009a, *PASP*, **121**, 1279

Steiner J. F., McClintock J. E., Remillard R. A., Narayan R., Gou L., 2009b, *ApJ*, **701**, L83

Tanaka Y., Lewin W. H. G., 1995, in *X-ray Binaries*. pp 126–174

Tanaka Y., et al., 1995, *Nature*, **375**, 659

Titarchuk L., 1994, *ApJ*, **434**, 570

Tomsick J. A., et al., 2014, *ApJ*, **780**, 78

Tomsick J. A., et al., 2018, *ApJ*, **855**, 3

Vadawale S. V., et al., 2016, In-orbit performance AstroSat CZTI. p. 99051G, doi:10.1117/12.2235373

Vaughan S., Edelson R., Warwick R. S., Uttley P., 2003, *MNRAS*, **345**, 1271

Verdhan Chauhan J., et al., 2017, *ApJ*, **841**, 41

Walborn N. R., 1973, *ApJ*, **179**, L123

Walton D. J., et al., 2016, *ApJ*, **826**, 87

Webster B. L., Murdin P., 1972, *Nature*, **235**, 37

Wilms J., Allen A., McCray R., 2000, *ApJ*, **542**, 914

Wilms J., Nowak M. A., Pottschmidt K., Pooley G. G., Fritz S., 2006, *A&A*, **447**, 245

Xiang J., Lee J. C., Nowak M. A., Wilms J., 2011, *ApJ*, **738**, 78

Yadav J. S., et al., 2016a, *ApJ*, **833**, 27

Yadav J. S., et al., 2016b, Large Area X-ray Proportional Counter (LAXPC) instrument onboard ASTROSAT. p. 99051D, doi:10.1117/12.2231857

Yamada S., Makishima K., Done C., Torii S., Noda H., Sakurai S., 2013, *PASJ*, **65**, 80

Zdziarski A. A., Johnson W. N., Magdziarz P., 1996, *MNRAS*, **283**, 193

Zhang S. N., Cui W., Chen W., 1997, *ApJ*, **482**, L155

Zhao X.-S., et al., 2020, *Journal of High Energy Astrophysics*, **27**, 53

Zhao X., et al., 2021, *ApJ*, **908**, 117

This paper has been typeset from a $\text{\TeX}/\text{\LaTeX}$ file prepared by the author.